Supplementary Information

A Solution-Processable Dissymmetric Porous Organic Cage

A. G. Slater,[a*] M. A. Little,[a] M. E. Briggs,[a] K. E. Jelfs,[b] A. I. Cooper[a]

[a]Department of Chemistry and Materials Innovation Factory, University of Liverpool, Crown Street, Liverpool, L69 7ZD. Email: anna.slater@liverpool.ac.uk
[b]Department of Chemistry, Imperial College London, South Kensington, London SW7 2AZ

This PDF file includes:

1. Materials and Methods

Materials: 1,3,5-Triformylbenzene was purchased from Manchester Organics and used as received. (±)-*trans*-1,2-Cyclohexanediamine was purchased from TCI and used as received. Other solvents were reagent or HPLC grade purchased from Fisher Scientific.

NMR: ^{1}H and ^{13}C spectra were recorded using an internal deuterium lock for the residual protons in $CDCl_3$ (δ = 7.26 ppm) at ambient probe temperature on a Bruker Avance 400 MHz NMR spectrometer.

HRMS: High resolution mass spectrometry was carried out using an Agilent Technologies 6530B accurate-mass QTOF Dual ESI mass spectrometer (capillary voltage 4000 V, fragmentor 225 V) in positive-ion detection mode. The mobile phase was MeOH + 0.1% formic acid at a flow rate of 0.25 mL/min.

TGA: Thermogravimetric analysis was carried out using a Q5000IR analyser (TA Instruments) with an automated vertical overhead thermobalance. All materials were desolvated by heating at 90 °C in a vacuum overnight prior to TGA analysis.

FTIR: Infra-red spectra were recorded using a Bruker Tensor 27 FTIR spectrometer with Quest ATR attachment (scans: 16 background, 32 sample).

PXRD: Laboratory powder X-ray diffraction data were collected in transmission mode on samples held on thin Mylar film in aluminium well plates on a Panalytical X'Pert PRO MPD equipped with a high throughput screening XYZ stage, X-ray focusing mirror and PIXcel detector, using Ni filtered Cu-Kα radiation. Data were measured over the range 4-50° in ~0.013° steps over 60 minutes. Le Bail fitting of PXRD data was collected on a powdered sample loaded in a borosilicate glass capillary in transmission geometry on a Panalytical Empyrean diffractometer producing Cu-*K*α radiation and equipped with an X-ray focussing mirror. Data were collected using a PIXcel 3D detector in 1D scanning mode. The pattern was indexed and lattice parameters extracted by Le Bail fitting using *TOPAS-Academic*.[1]

SEM: Scanning electron microscopy images were obtained using a Hitachi S-4800 cold Field Emission Scanning Electron Microscope (FE-SEM). Scanning-mode samples were prepared by depositing dry crystals on 15 mm Hitachi M4 aluminium subs using an adhesive high-purity carbon tab before coating with a 2 nm layer of gold using an Emitech K550X automated sputter coater. Imaging was conducted at a working distance of 8 mm and a working voltage of 3 kV using a mix of upper and lower secondary electron detectors. The FE-SEM measurement scale bar was calibrated using certified SIRA calibration standards.

Gas Sorption Analysis: Surface areas were measured by nitrogen sorption at 77.3 K. Powder samples were degassed offline at 90 °C for 15 h under dynamic vacuum (10^{-5} bar) before analysis, followed by degassing on the analysis port under vacuum, also at 90 °C. Gas sorption isotherms for N_2, H_2, CO_2, Xe, and Kr were measured using Micromeritics 3flex, 2020, or 2420 volumetric adsorption analyser at the temperatures specified on the gas sorption plots.

Single crystal XRD: Single crystal X-ray data sets were measured on a Rigaku MicroMax-007 HF rotating anode diffractometer (Mo-Kα radiation, λ = 0.71073 Å, Kappa 4-circle goniometer, Rigaku Saturn724+ detector). A solvated single crystal, isolated from the crystallization solvent, was mounted directly on a MiTeGen gripper and flash cooled under a dry nitrogen gas flow. Rigaku frames were converted to Bruker compatible frames using the programme ECLIPSE.[2] Empirical absorption corrections, using the multi-scan method, were performed with the program SADABS.[3] Structures were solved with by direct methods using SHELXS,[4] and refined by full-matrix least squares on $|F|^2$ by SHELXL,[5] interfaced through the programme OLEX2.[6] Unless stated all non-H-atoms were refined anisotropically, and unless stated H-atoms were fixed in geometrically estimated positions and refined using the riding model. Supplementary CIF's, that include structure factors and responses to checkCIF alerts, are available free of charge from the Cambridge Crystallographic Data Centre (CCDC) via www.ccdc.cam.ac.uk/data_request/cif.

Solubility testing: The procedure developed for solubility screening of scrambled cages in chloroform was followed.[7] Cage sample (desolvated in a vacuum oven at 90 °C overnight) was diluted with $CHCl_3$ (pre-treated with anhydrous K_2CO_3 overnight) until a saturated solution formed. The saturated solution was stirred at rt for 2 hours to ensure no further cage dissolved before being filtered through a 0.2 µm PTFE syringe filter. A 100 µL sample was added to a pre-weighed vial, followed by a 100 µL $CHCl_3$ syringe wash. Samples had $CHCl_3$ removed under an N_2 flow before being dried in the vacuum oven at 90 °C overnight. Samples of cage were then reweighed to enable calculation of solubility in terms of mg/mL.

2. Experimental Details and Characterisation

2.1 Initial synthesis of CC3-*RS*/CC3-*SR*, using conditions reported for CC3-*R*

1,3,5-Triformylbenzene (TFB, 500 mg, 3.08 mmol) was suspended in DCM (25 mL) to afford a white suspension. (±)-*trans*-1,2-Cyclohexanediamine (528 mg) was dissolved in DCM (25 mL) and carefully layered onto the TFB suspension at RT without stirring. After 48 hours, the TFB was seen to dissolve, and a precipitate was seen to form at the surface of the solution. The solid (408 mg, 0.36 mmol, 46.8%, identified via PXRD as **CC3-*R*/CC3-*S***, see **Fig 4bii** in main paper) was separated from the soluble products via filtration through glass fibre filter paper. The filtrate was concentrated to ~ 10 mL at RT, hexane (20 mL) was charged with stirring and the resulting white precipitate collected via suction filtration to yield pure product (312 mg, 0.28 mmol, 36.2%). ^{1}H NMR (400MHz, $CDCl_3$) δ = 8.39 (t, *J* = 1.6 Hz, 3 H), 8.21 (s, 3 H), 8.17 (s, 6 H), 8.12 (s, 3 H), 7.92 (t, *J* = 1.5 Hz, 3 H), 7.76 (s, 3 H), 7.18 (t, *J* = 1.5 Hz, 3 H), 3.51 - 3.28 (m, 12 H), 1.90 - 1.83 (m, 24 H), 1.65 - 1.69 (m, 12 H), 1.56 - 1.38 (m, 12 H). ^{13}C NMR (400MHz, $CDCl_3$) δ = 160.09, 159.62, 159.57, 158.89, 136.99, 136.93, 136.49, 136.13, 135.14, 130.08, 128.78, 124.08, 75.90, 75.07, 74.46, 73.59, 33.29, 33.13, 32.49, 24.42. MS (HRMS)$^+$ calcd for $C_{72}H_{85}N_{12}$ $[M+H]^+$: 1117.7020; found 1117.7027 $[M+H]^+$, 559.3558 $[M+2H]^{2+}$, 373.2391 $[M+3H]^{3+}$

2.1.1 Elucidation of structure from NMR

Mass spectrometry confirmed that the mass of the new isolated cage is the same as homochiral **CC3**, strongly suggesting that the material is an isomer of **CC3** despite its very different NMR. Homochiral **CC3** is symmetrical, and hence has a simple NMR spectrum with a single peak for aromatic protons at 7.90 ppm in $CDCl_3$, and a single imine peak at 8.16 ppm. In the case of the new cage, 3 imine peaks (8.21, 8.17, 8.12 ppm integrating to 3, 6, and 3 protons respectively), and 4 peaks resulting from aromatic protons (8.39, 7.92, 7.76, 7.18 ppm, all integrating to 3 protons) could be distinguished. In the ^{13}C spectrum, 4 imine peaks, 4 aromatic C-H peaks, and 4 aromatic quaternary C peaks can be discerned when corroborated with HSQC and APT data. Thus, we hypothesised there was one symmetrical triiminobenzene (TIB) moiety and three asymmetric TIB moieties within the cage (**Fig S1**), resulting from the orientation of the imine bonds in the cage structure, which results from the different stereochemistry of cyclohexyldiimine moieties present (one TIB is bound to three CHDA moieties with the same chirality; three TIB are bound to two CHDA moieties of one chirality, and one of the opposite chirality). This was unambiguously confirmed by SCXRD.

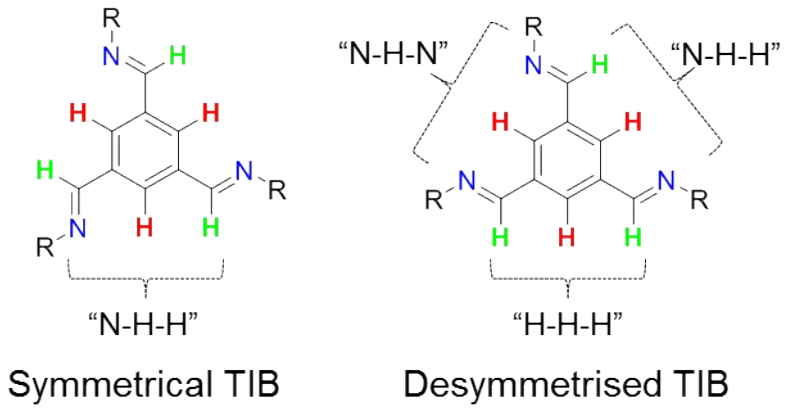

Figure S1: Symmetrical (left) and desymmetrised (right) triiminobenzene (TIB) units. Four symmetrical TIB moities are present in homochiral CC3; in CC3-RS, one symmetrical TIB and three asymmetric TIB moieties are present. Nitrogen atoms shown in blue; aromatic protons shown in red, and imine protons shown in green.

2.2 Investigation of effect of conditions on production of isomers of CC3

The effect of temperature (entry 6-8), concentration (entry 1,2,6,9), stirring (entry 3), scale (entry 3-5), ratio of *R,R*- and *S,S*-CHDA (entry 10-13), and absence of TFA (entry 14) were investigated (**Table S1**). The most reproducible conditions with the shortest reaction time were found to be: room temperature, 2.5 mg/mL concentration with respect to TFB, with stirring, using a ratio of 1:1 *R,R*-CHDA:*S,S*-CHDA, and with addition of TFA. Products in solution were characterised by ^1H NMR; aliquots were taken at the times specified in the table, dried with a stream of N_2, then dissolved in $CDCl_3$ without further purification or filtration to remove insoluble material. As aliquots were also taken throughout the reactions, accurate yield calculations were not possible.

Table S1: Optimisation of reaction conditions for CC3-*RS* and CC3-*SR*

Entry	TFB:*R,R*-CHDA:*S,S*-CHDA	Concentration TFB mg/mL	TFA	Temp	Stirring	Products in solution	White precipitate	NMR
1[a]	4:3:3 24 mg TFB	5 mg/mL†	Yes	RT	No	24h: CC3-RS	Yes	As Fig S8
2[a]	4:3:3 200 mg TFB	10 mg/mL	Yes	RT	No	24 h: CC3-RS, TFB	Yes	Not shown
3[a]	4:3:3 200 mg TFB	10 mg/mL	Yes	RT	Yes	24 h: CC3-RS TFB	Yes	Not shown
4[a]	4:3:3 500 mg TFB	10 mg/mL	Yes	RT	No	24h: TFB + CC3-RS 48h: CC3-RS + trace TFB	Yes	Not shown
5[a] (repeat of 4)	4:3:3 500 mg TFB	10 mg/mL	Yes	RT	No	24 h: CC3-RS + TFB	Yes	Not shown
6	4:3:3 203 mg TFB	4 mg/mL	Yes	RT	Yes	5h: CC3-RS	Yes	Fig S2
7	4:3:3 203 mg TFB	4 mg/mL	Yes	0 °C	Yes	5h: CC3-RS + complex cage products	Yes	Fig S2
8	4:3:3 203 mg TFB	4 mg/mL	Yes	-42 °C	Yes	5h: very complex spectrum	Yes	Fig S2
9	4:3:3 200 mg TFB	2.5 mg/mL	Yes	RT	Yes	5h: CC3-RS	Yes	Fig S3/4
10-1, 10-2	4:5:1 50 mg TFB	2.5 mg/mL	Yes	RT	Yes	CC3-R, CC3-RS, TFB, complex products	Yes	Fig S5/6

11-1, 11-2	4:4:2 50 mg TFB	2.5 mg/mL	Yes	RT	Yes	CC3-R, CC3-RS	Yes	Fig S5/6
12-1, 12-2	4:2:4 50 mg TFB	2.5 mg/mL	Yes	RT	Yes	CC3-S, CC3-RS	Yes	Fig S5/6
13-1, 13-2	4:1:5 50 mg TFB	2.5 mg/mL	Yes	RT	Yes	CC3-S, CC3-RS	Yes	Fig S5/6
14	4:3:3 100 mg TFB	4 mg/mL	No	RT	Yes	Complex NMR	No	Not shown

[a] Using procedure described in 2.1; yields in 2.1 are for entry 5. †Note; 4mg/mL is the saturation concentration for TFB; any concentration above this has a proportion of suspended TFB.

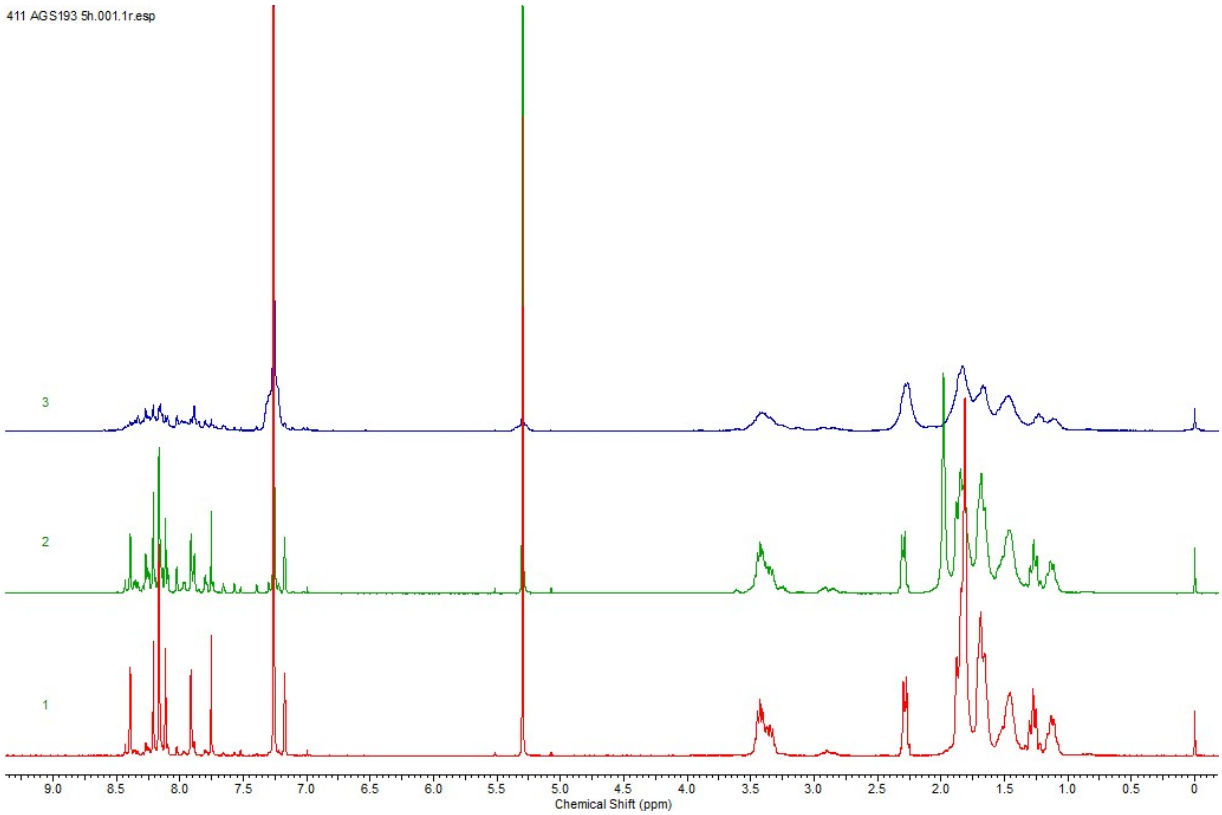

Figure S2: ^{1}H NMR of entries 6 (red), 7 (green), 8 (blue) after 5 hours

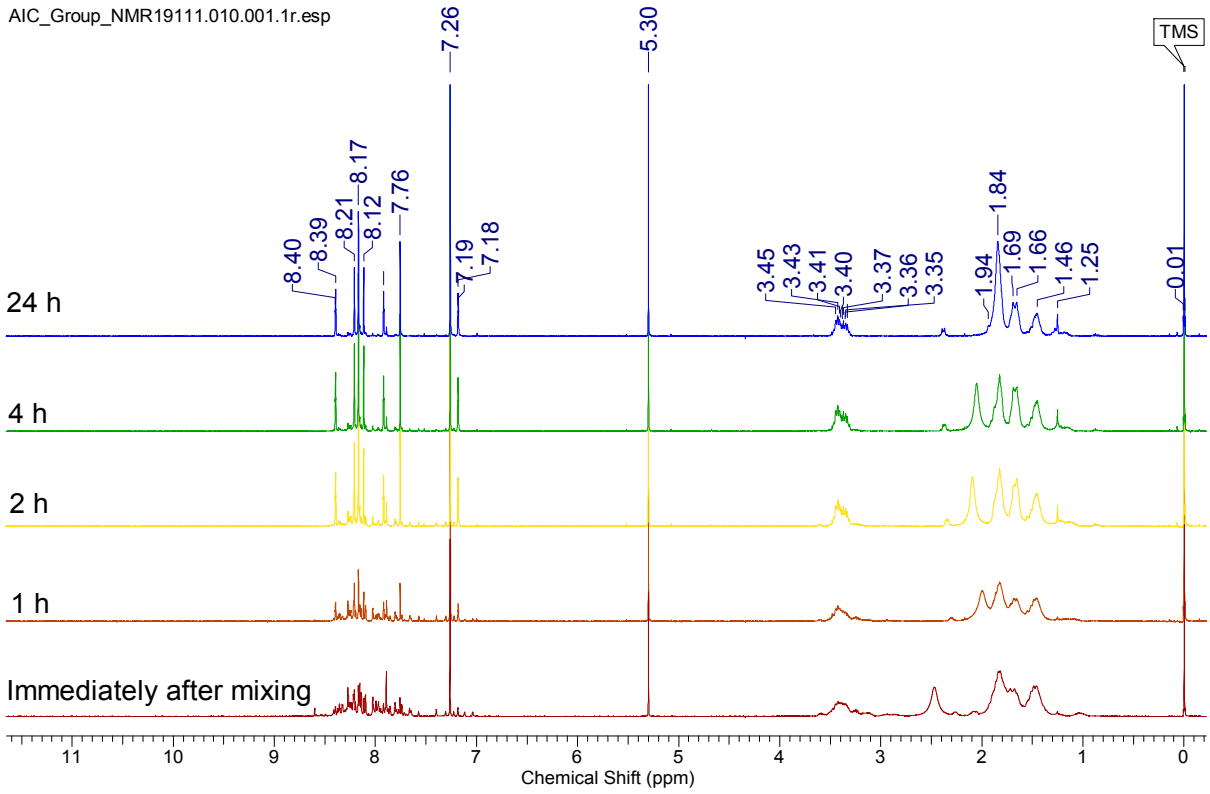

Figure S3: ^{1}H NMR in $CDCl_3$ of aliquots of a reaction (entry 9 from **Table S1**) in progress to form **CC3**-*RS* and **CC3**-*SR* in DCM. Aliquots were taken immediately after mixing (red), then after 1 (orange), 2 (yellow), 4 (green) and 24 hours (blue).

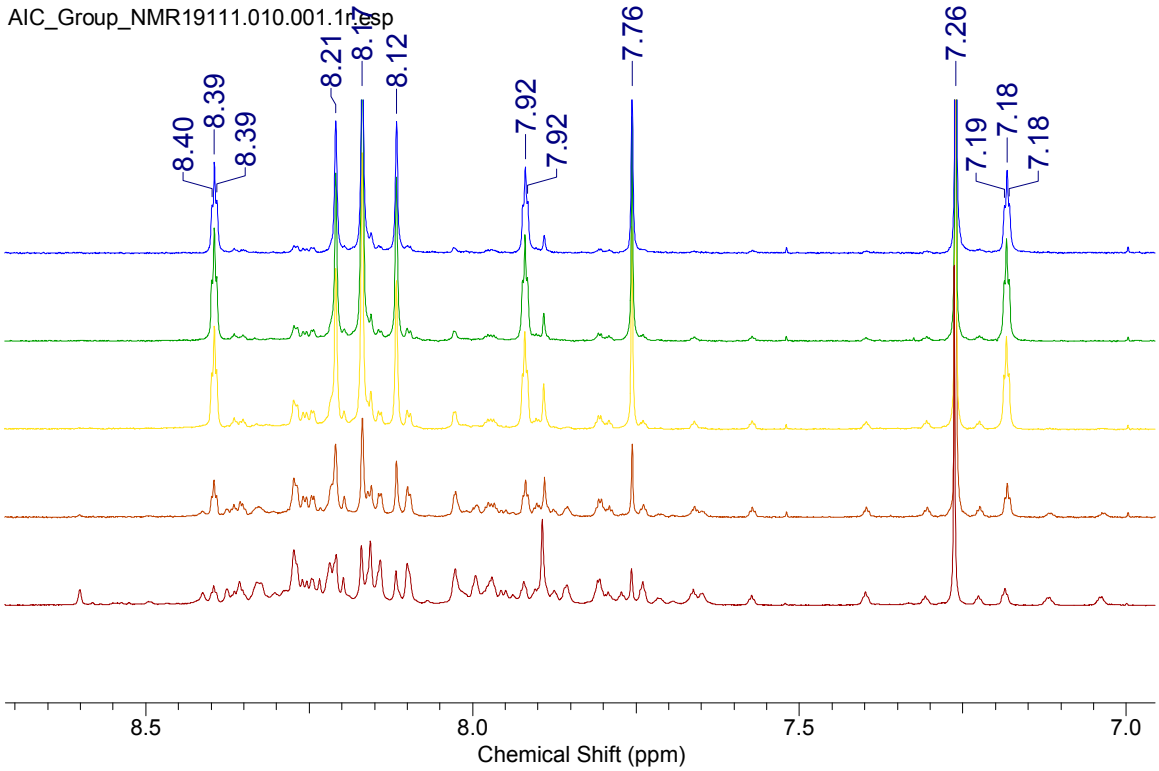

Figure S4: Spectra shown in previous figure**,** zoomed in to show aromatic and imine region (8.7 - 7.0 ppm).

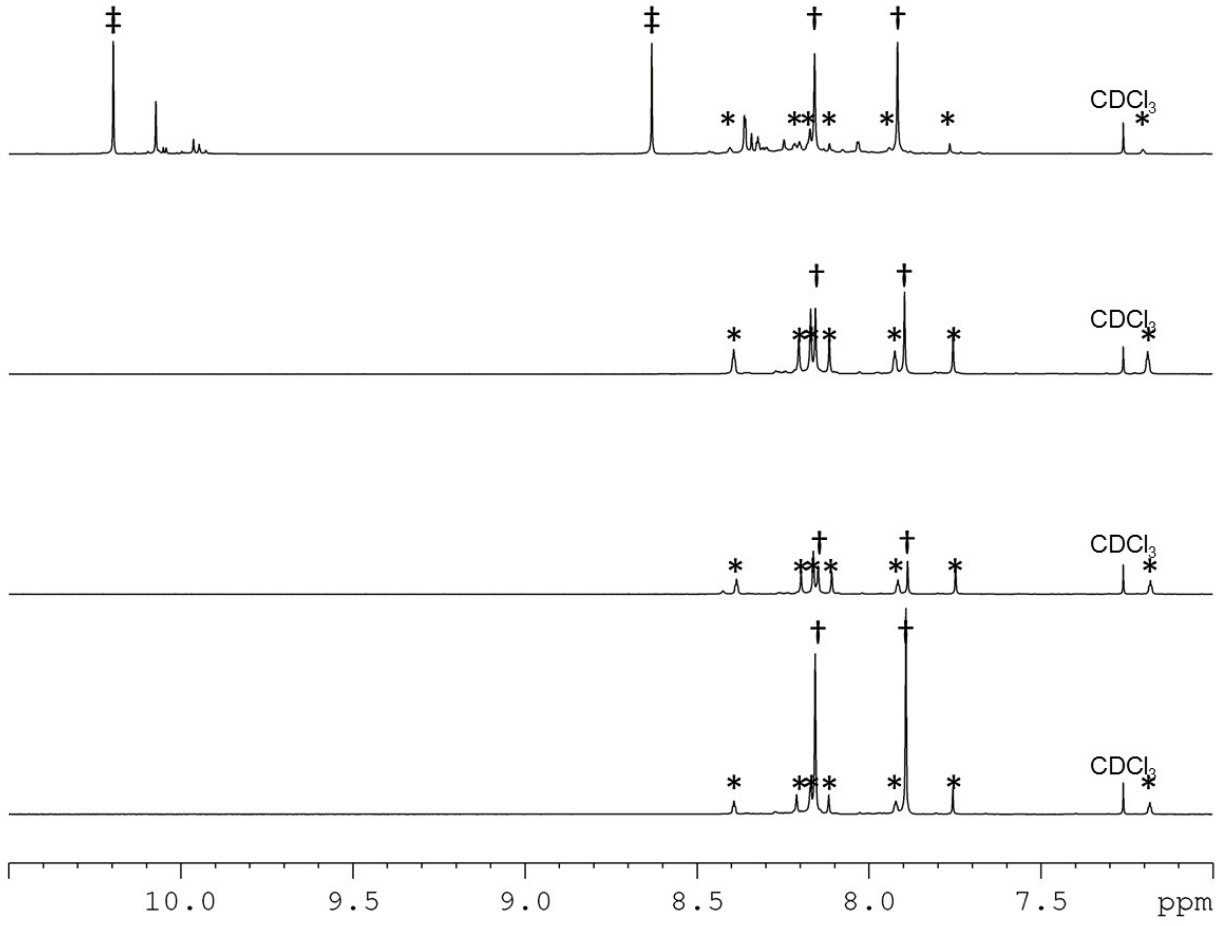

Figure S5: ^{1}H NMR of entries (bottom to top) 10-1, 11-1, 12-1, 13-1, zoomed in to show 10.5 – 7.0 ppm. Asterisks indicate peaks corresponding to **CC3**-*RS* and **CC3**-*SR*; daggers indicate peaks corresponding to homochiral **CC3**. In the case of 10-1, two sharp peaks indicated by double daggers can also be seen at 10.2 and 8.7 which correspond to TFB starting material. The other peaks in 10-1 are presumed to be related to mono- and di-substituted TFB derivatives. Relative integrations of the peaks for each cage could not be accurately determined due to peak overlap.

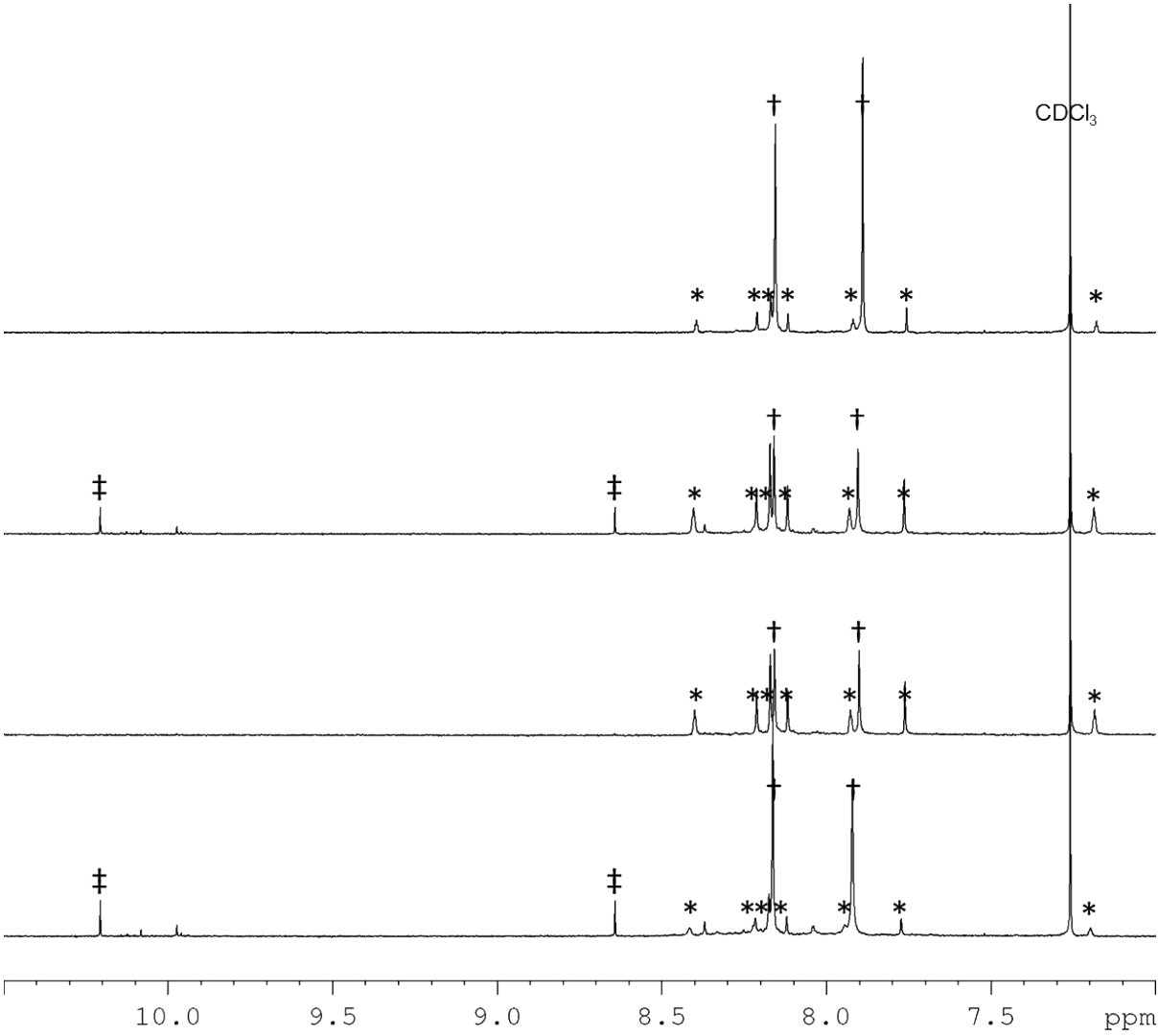

Figure S6: ^{1}H NMR of entries (bottom to top) 10-2, 11-2, 12-2, 13-2, zoomed in to show 10.5 – 7.0 ppm. Asterisks indicate peaks corresponding to **CC3**-*RS* and **CC3**-*SR*; daggers indicate peaks corresponding to homochiral **CC3**. Double daggers indicate peaks corresponding to TFB starting material. Relative integrations of the peaks for each cage could not be accurately determined due to peak overlap.

2.3 Modified synthesis of CC3-*RS*/CC3-*SR*

1,3,5-Triformylbenzene (TFB, 200 mg, 1.23 mmol) was suspended in DCM (80 mL) to afford a clear solution. (±)-*trans*-1,2-Cyclohexanediamine (528 mg) was dissolved in DCM (25 mL) and added to the first solution at RT with stirring. After 24 hours, the solution had turned cloudy. The solid was separated from the soluble products via filtration through glass fibre filter paper. The filtrate was concentrated to ~ 10 mL at RT, hexane (20 mL) was charged with stirring and the resulting white precipitate collected via suction filtration to yield pure product (117 mg, 0.15 mmol, 34.1%), characterisation as above.

2.4 NMR Spectroscopy

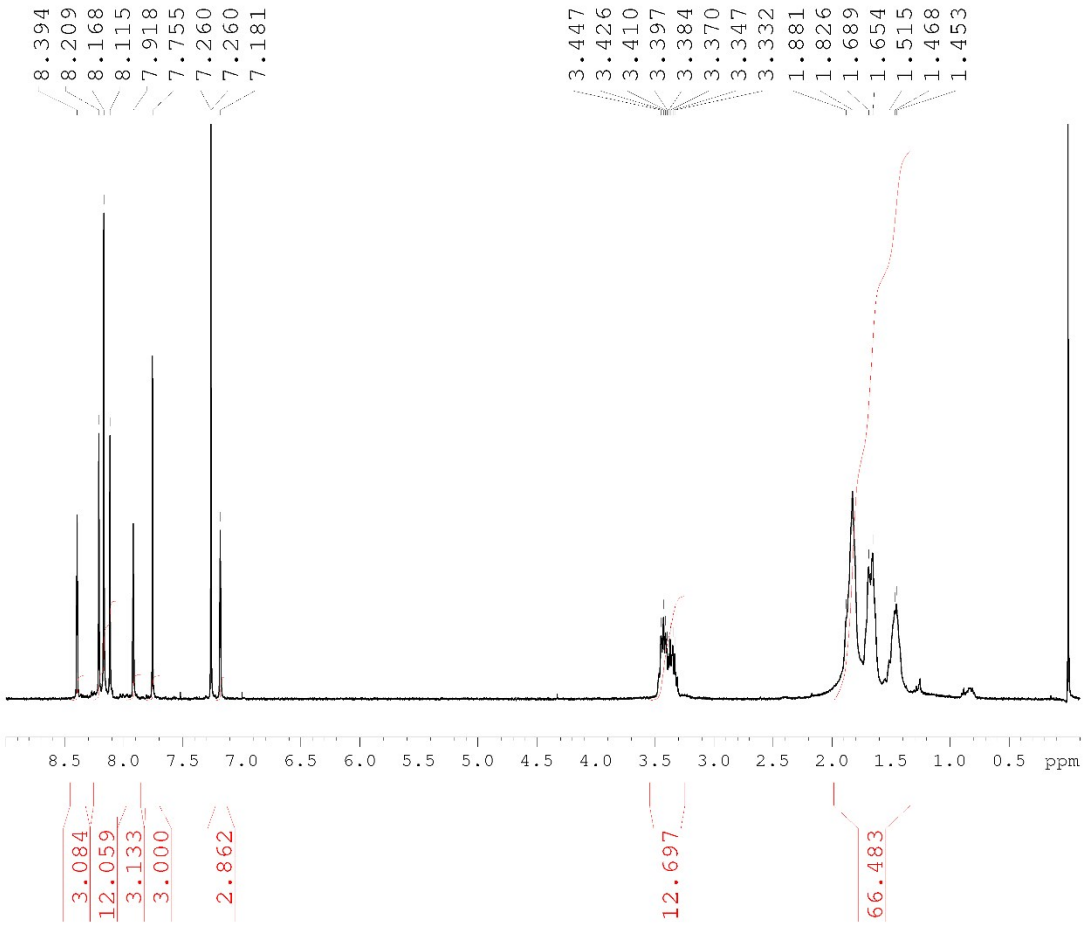

Figure S7: ^{1}H NMR of **CC3**-*RS* and **CC3**-*SR* in $CDCl_3$

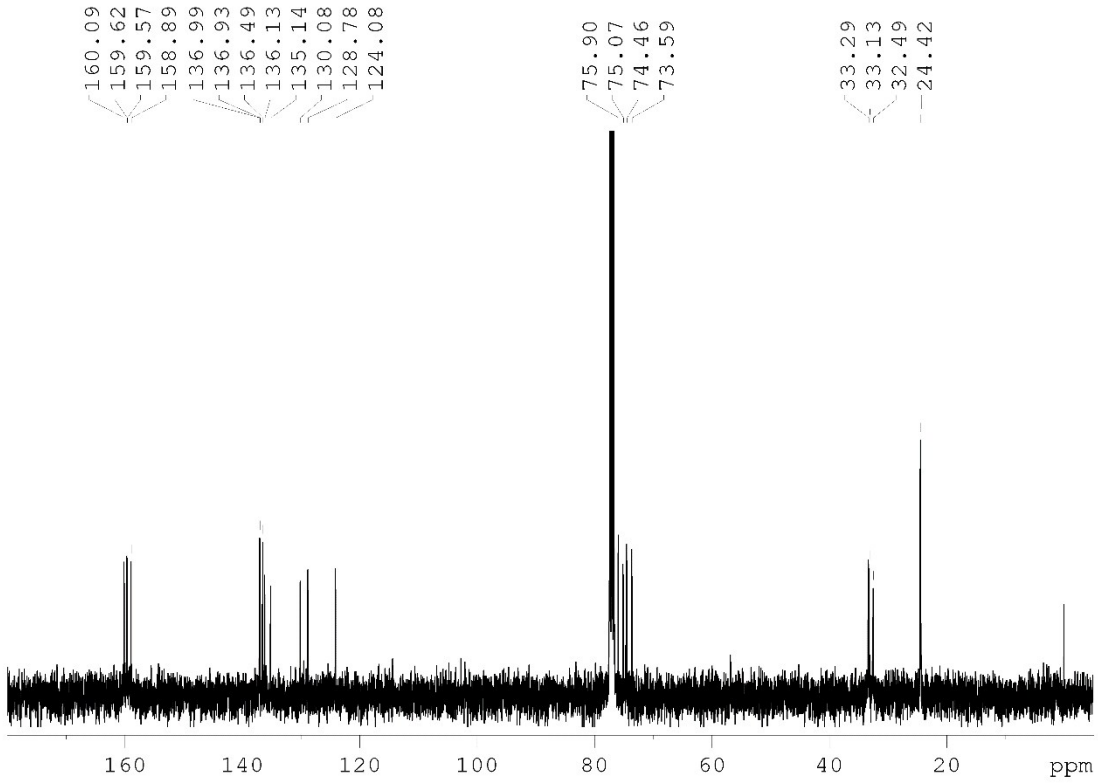

Figure S8: ^{13}C NMR of **CC3**-*RS* and **CC3**-*SR* in $CDCl_3$

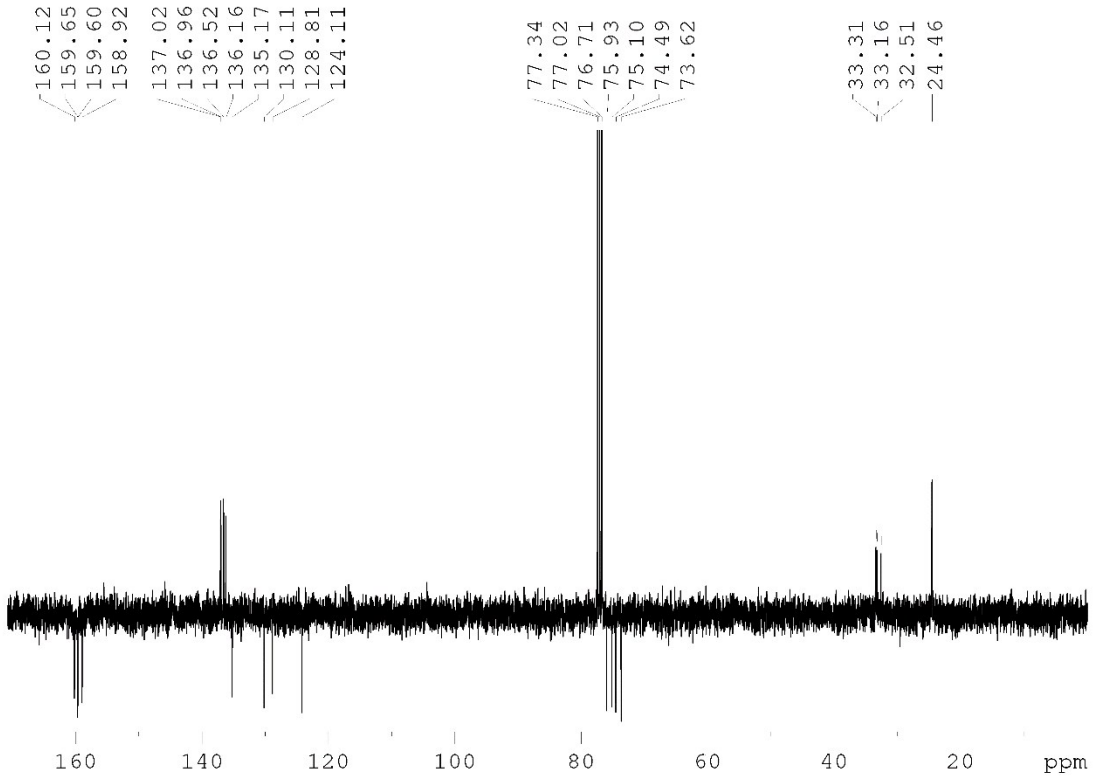

Figure S9: ^{13}C APT NMR of **CC3**-*RS* and **CC3**-*SR* in $CDCl_3$. Note that in this experiment, CH and CH_3 peaks are negative, and quaternary C and CH_2 peaks are positive, as seen for the $CDCl_3$ solvent peak at 77.0 ppm.

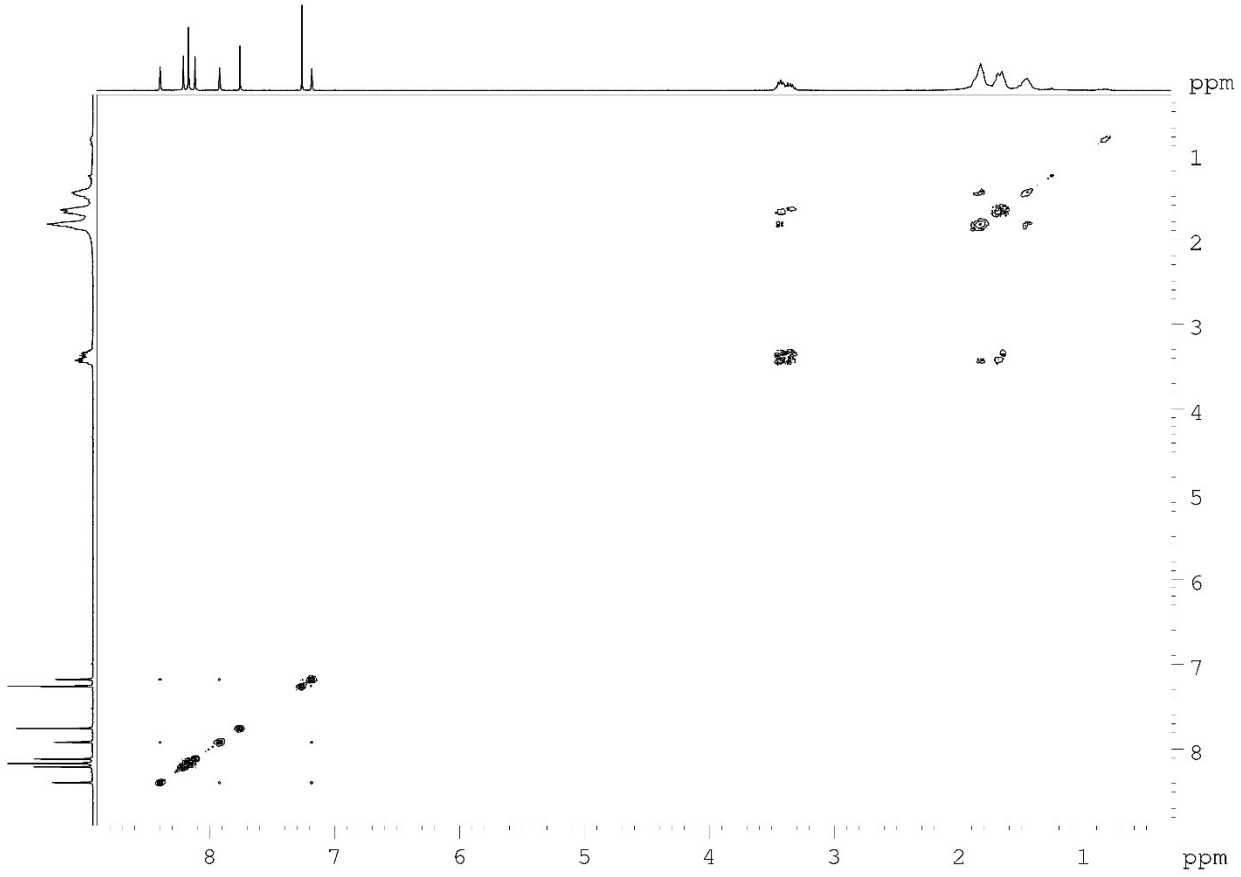

Figure S10: 2D COSY NMR of **CC3**-*RS* and **CC3**-*SR* in $CDCl_3$

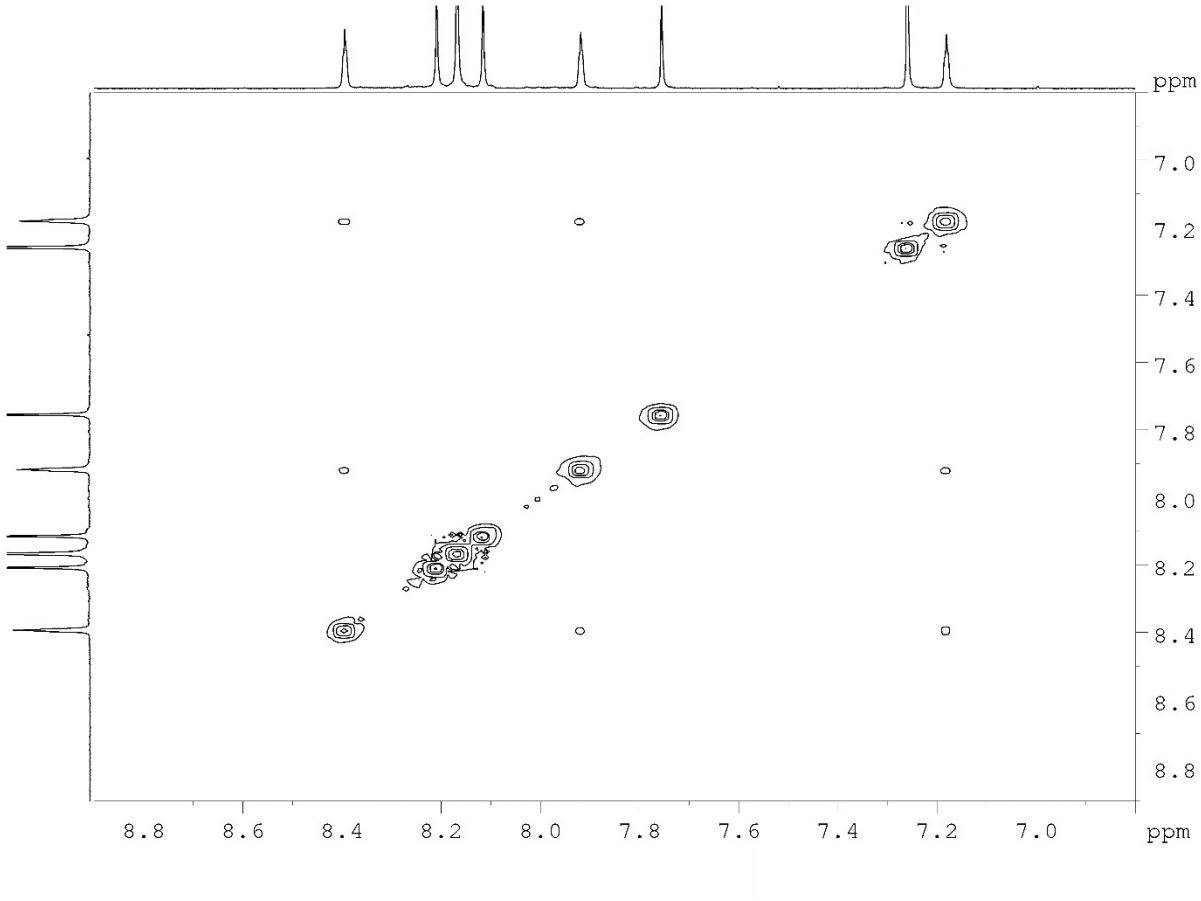

Figure S11: 2D COSY NMR of **CC3**-*RS* and **CC3**-*SR* in $CDCl_3$, zoomed in to show aromatic and imine region (6.8 - 8.9 ppm)

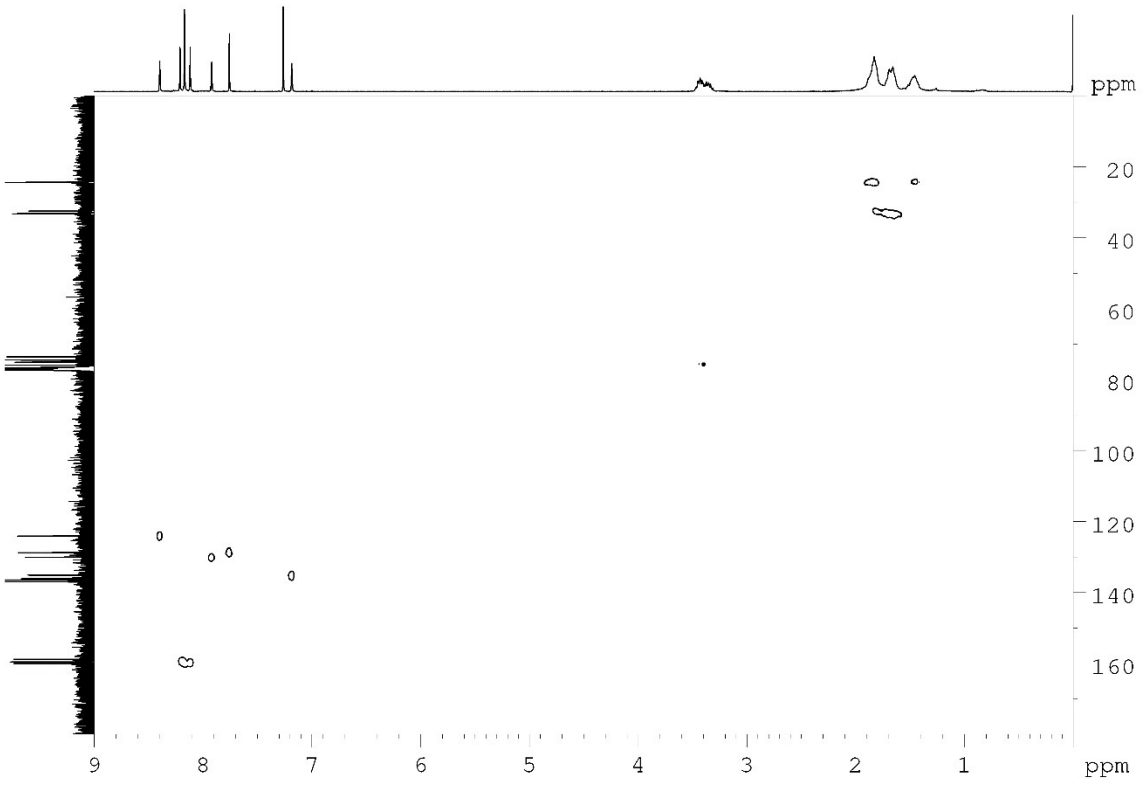

Figure S12: 2D HSQC NMR of **CC3**-*RS* and **CC3**-*SR* in $CDCl_3$

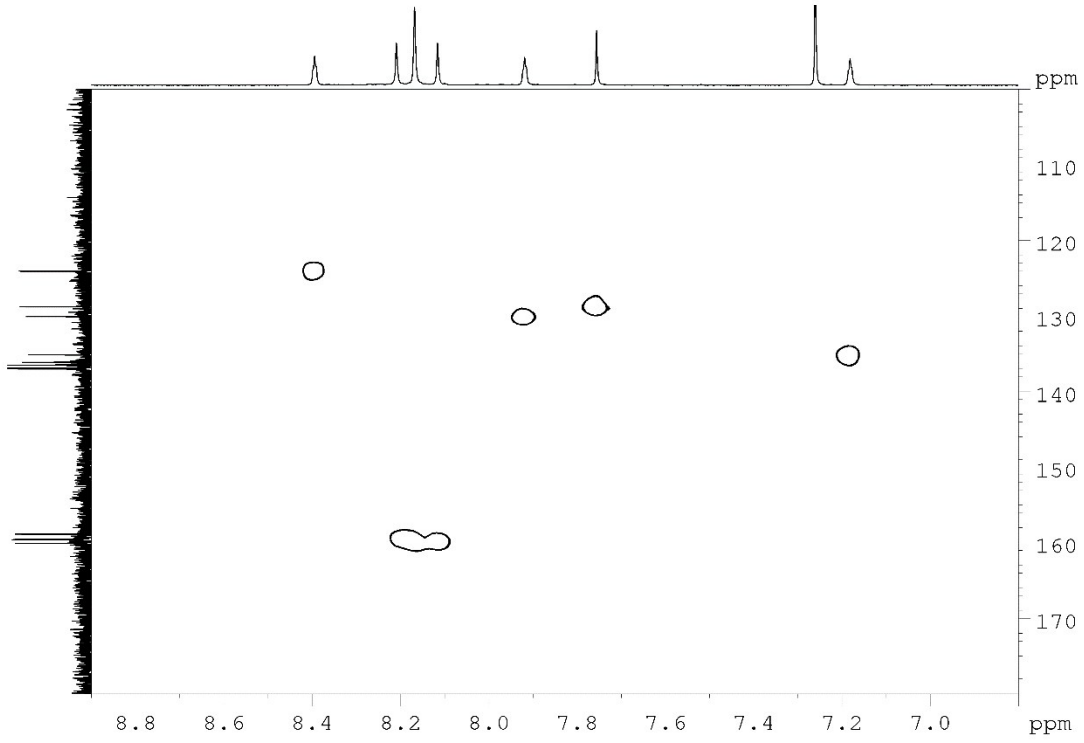

Figure S13: 2D HSQC NMR of **CC3**-*RS* and **CC3**-*SR* in $CDCl_3$ zoomed in to show aromatic and imine region (6.8 - 8.9 ppm on x axis, 100 – 180 ppm on y axis)

2.5 Stability of CC3-RS/CC3-SR in solution

To assess the solution phase stability of **CC3**-*RS*/**CC3**-*SR*, the cage (100 mg) was taken up in DCM (50 mL) and split between two round bottomed flasks (**Figure S14**). TFA (1 drop) was added to the right-hand flask (**Figure S14**) and the solutions were stirred at RT for 6 days. After 6 days, aliquots were taken from each, dried under a stream of N_2, dissolved in $CDCl_3$ and analysed by NMR without further purification (**Figure S15/16**). NMR analysis of **CC3**-*RS*/**CC3**-*SR* stirred with DCM for 6 days showed no change to the parent cage: ^{1}H NMR (400 MHz, $CDCl_3$) δ 8.39 (s, 3H), 8.21 (s, 3H), 8.17 (s, 6H), 8.12 (s, 3H), 7.92 (s, 3H), 7.76 (s, 3H), 3.41 (m, 12H), 1.85 (m, H), 1.65 (m, H), 1.45 (t, J = 9.4 Hz, 3H), **Figure S15**). NMR analysis of CC3-RS/CC3-SR stirred with DCM in the presence of TFA for 6 days showed that the only aromatic compounds remaining in solution were TFB and partially substituted TFB (**Figure S16**). PXRD of the insoluble precipitate was poorly crystalline and could not be identified.

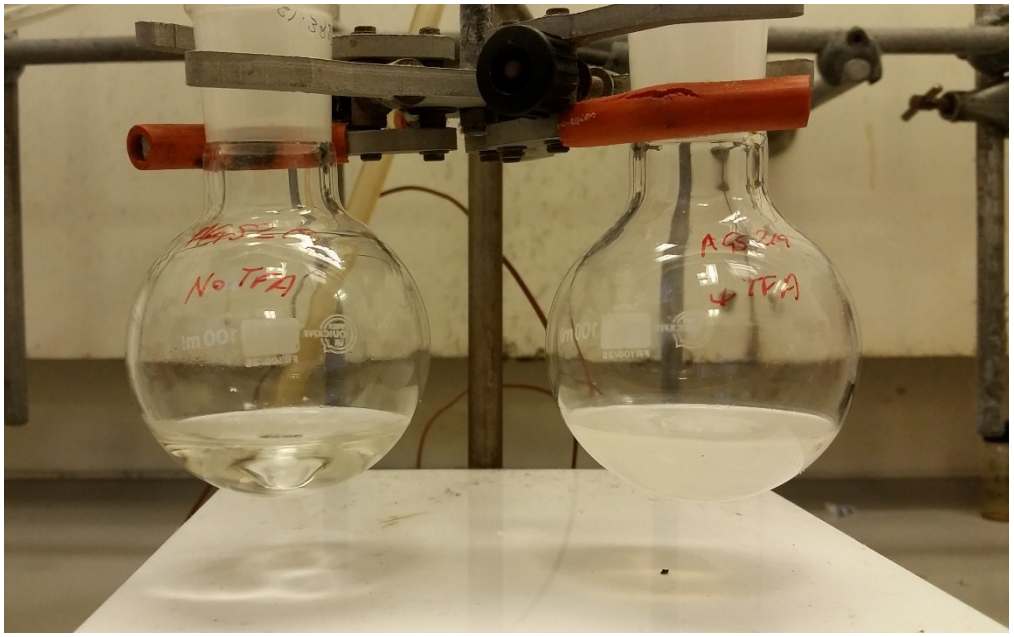

Figure S14. Image showing the two solutions of **CC3**-*RS*/**CC3**-*SR* with (right) and without (left) added TFA. The solution with TFA was observed to turn cloudy.

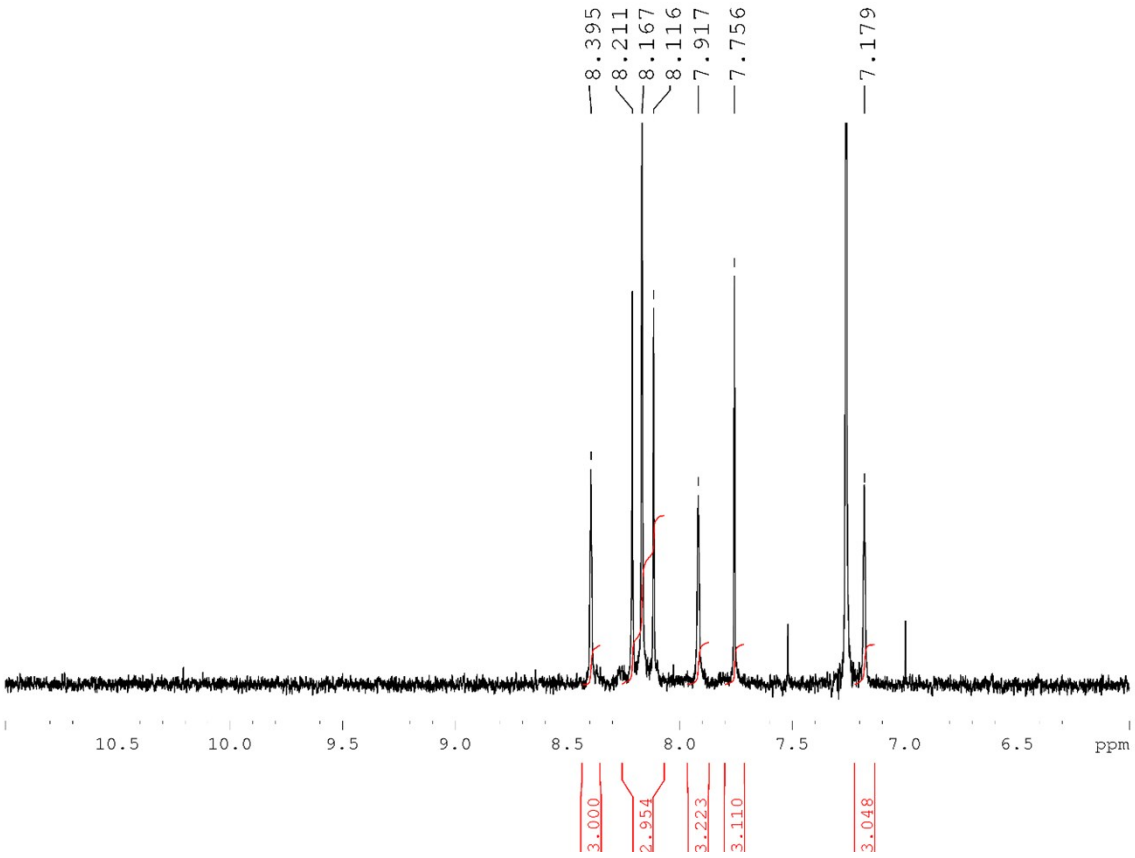

Figure S15. NMR spectrum of **CC3**-*RS*/**CC3**-*SR* after stirring in DCM for 6 days, zoomed to show aromatic and imine region (11 – 6 ppm).

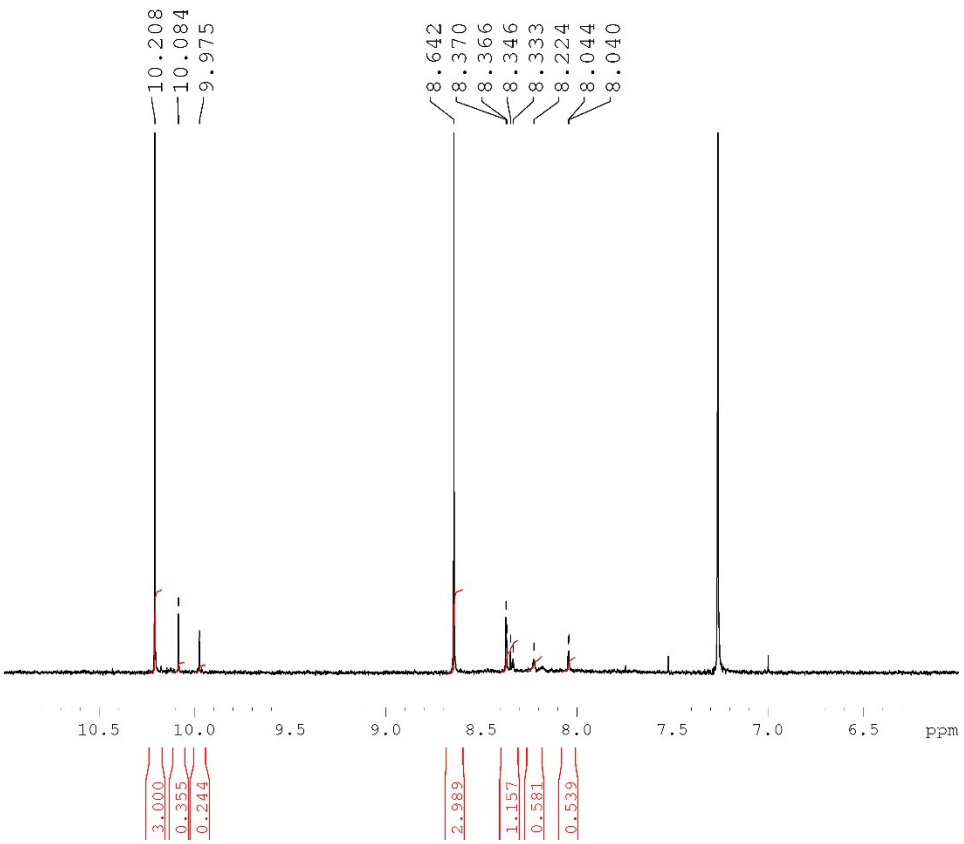

Figure S16. NMR spectrum of **CC3**-*RS*/**CC3**-*SR* after stirring in DCM in the presence of TFA for 6 days, zoomed to show aromatic and imine region (11 – 6 ppm).

2.6 Thermogravimetric Analysis

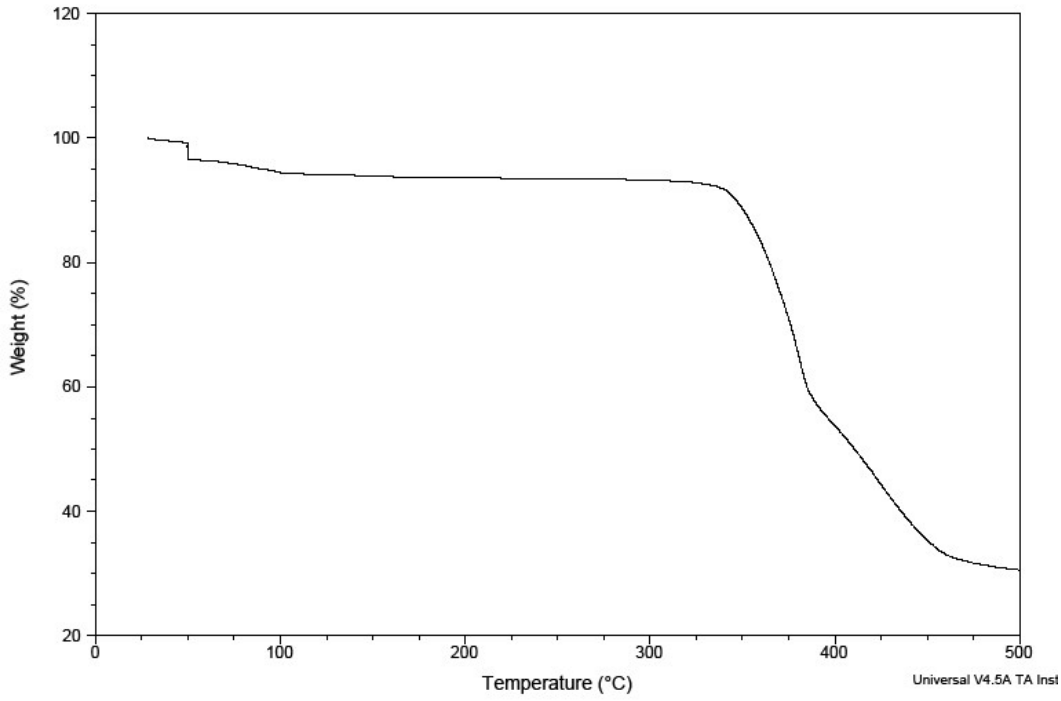

Figure S17: TGA plot for **CC3**-*RS*/**CC3**-*SR*. The TGA method was as follows: ramp 5.00 °C/min to 50.00 °C; isothermal at 50.00 °C for 30 minutes; ramp 5.00 °C/min to 100.00 °C; isothermal for 30.00 minutes; ramp 5.00 °C/min to 500.00 °C.

2.7 Infrared Spectroscopy

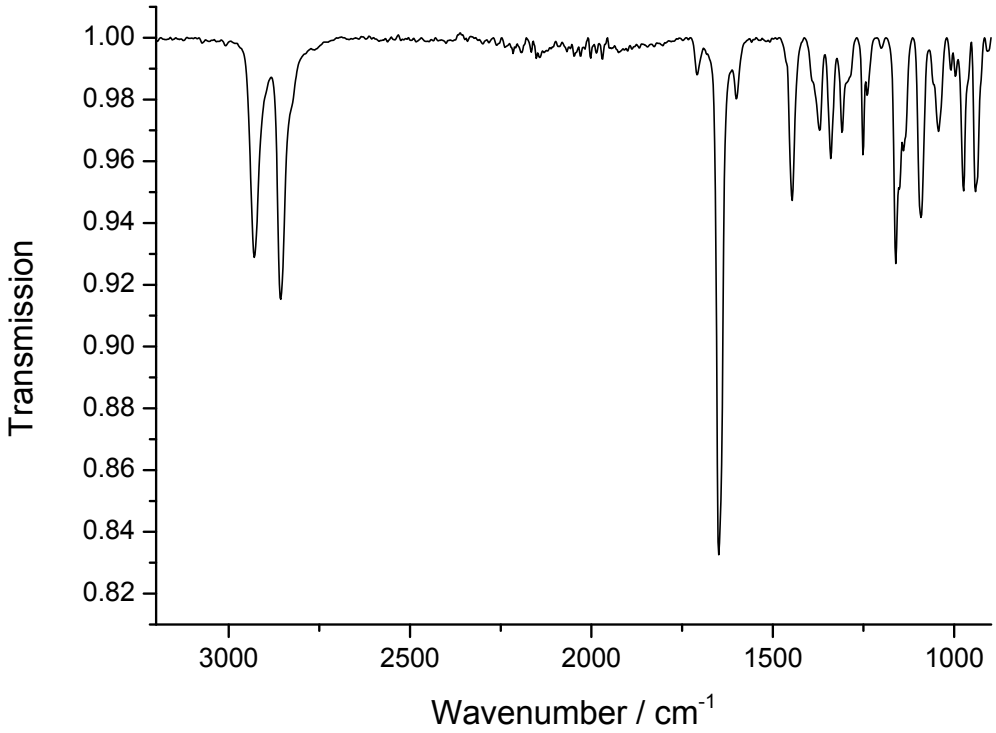

Figure S18. FTIR spectroscopy (ATR) of **CC3-*RS*/CC3-*SR***

2.8 Single Crystal X-ray Crystallography

Crystal data for **CC3-*RS*/CC3-*SR***; ***R,R,R,S,S,S*-CC3**·0.77(CH_2Cl_2)·0.32(MeOH)·1.57(H_2O). CCDC n. 1571867. Formula $C_{73.1}H_{89.96}Cl_{1.55}N_{12}O_{1.89}$; M = 1221.97 g·mol^{-1}; trigonal space group $R\bar{3}$, colourless crystal; a = 24.4830(11), c = 19.6123(9) Å; V = 10180.9(10) Å^3; ρ = 1.196 g·cm^{-3}; μ = 0.132 mm^{-3}; F (000) = 3924; crystal size = 0.14 x 0.13 x 0.03 mm^3; T = 100(2) K; 31027 reflections measured (1.414 < θ < 26.368°), 4632 unique (R_{int} = 0.0579), 3961 (I > 2σ(I)); R_1 = 0.0608 for observed and R_1 = 0.0731 for all reflections; wR_2 = 0.1666 for all reflections; max/min residual electron density = 0.598 and -0.366 e·Å^{-3}; data/restraints/parameters = 4632/18/281; GOF = 1.124. The crystal structure was refined with the TWINLAW [010 100 00] and BASF refined to 0.4879(19). Solvent was poorly ordered in the intrinsic cage cavity and window site. Solvent in the intrinsic cavity was modelled as CH_2Cl_2 and this molecule was refined with restrained displacement parameters (RIGU and ISOR in SHELX). Disordered electron density in the window site was modelled as partially occupied MeOH and H2O. The MeOH molecule was refined with restrained displacement parameters (RIGU in SHELX). For a displacement ellipsoid plot, see **Fig S19**.

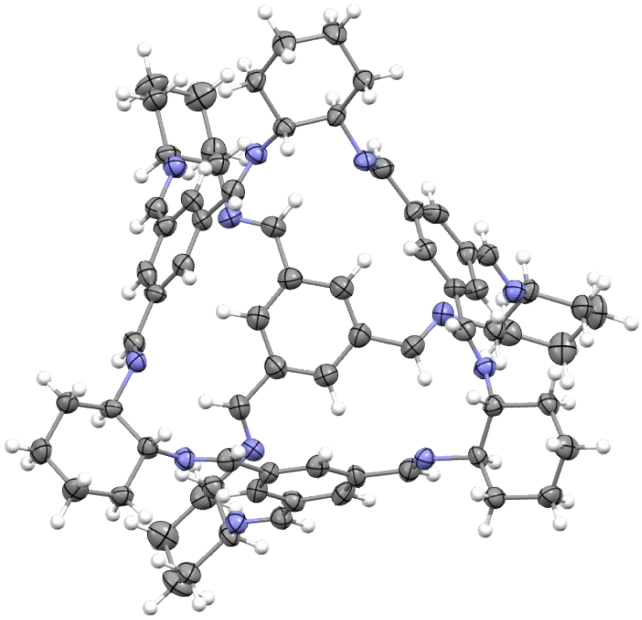

Figure S19. Displacement ellipsoid plot from the solvated single crystal structure of **CC3**-*RS*/**CC3**-*SR* showing one *R,R,R,S,S,S*-**CC3** cage in entirety. Solvent molecules omitted for clarity. Ellipsoid displayed at 50 % probability level.

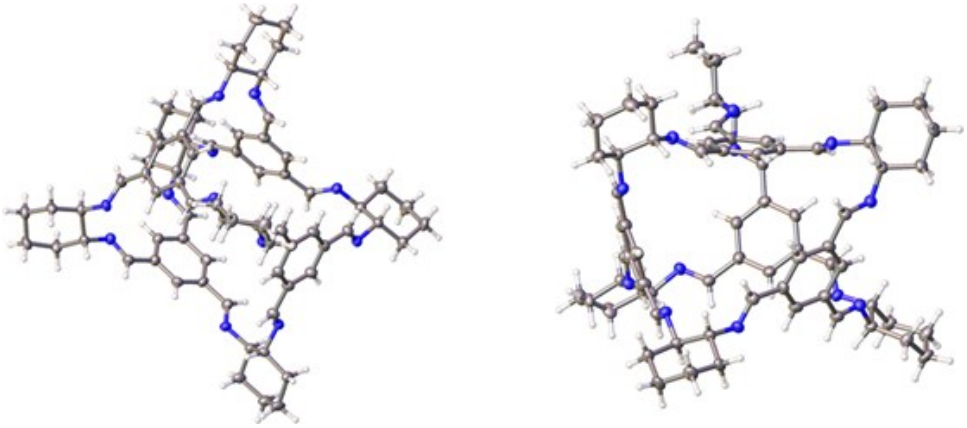

Figure S20. Displacement ellipsoid plot from the solvated single crystal structure of **CC3**-*RS*/**CC3**-*SR*; showing arrangement of aromatic rings. Two views show; ellipsoids displayed at 50 % probability level; solvent omitted for clarity.

The single crystal, refined as *R,R,R,S,S,S*-**CC3**·0.77(CH_2Cl_2)·0.32(MeOH)·1.57(H_2O), was thermally desolvated under a dry nitrogen gas stream at 400 (50 K/hr ramp rate) before a second data collection was recorded. At 400 K no solvent molecules could be located in the difference map.

Crystal data for desolvated **CC3**-*RS*/**CC3**-*SR*; *R,R,R,S,S,S*-**CC3**. CCDC n. 1571866. Formula $C_{72}H_{84}N_{12}$; M = 1117.51 g·mol^{-1}; trigonal space group R , colourless crystal; a = 24.741(5), c = 19.826(4) Å; V = 10510(5) Å^3; ρ = 1.059 g·cm^{-3}; μ = 0.064 mm^{-3}; F (000) = 3600; crystal size = 0.14 x 0.131 x 0.025 mm^3; T = 400(2) K; 26156 reflections measured ($1.646 < \theta < 20.823°$), 2458 unique (R_{int} = 0.0558), 2137 ($I > 2\sigma(I)$); R_1 = 0.0538 for observed and R_1 = 0.0629 for all reflections; wR_2 = 0.1513 for all reflections; max/min residual electron density = 0.243 and -0.133 e·Å^{-3}; data/restraints/parameters = 2458/0/254; GOF = 1.075. The crystal structure was refined with the TWINLAW [010 100 00] and BASF refined to 0.483(3). For a displacement ellipsoid plot, see **Fig. S21**.

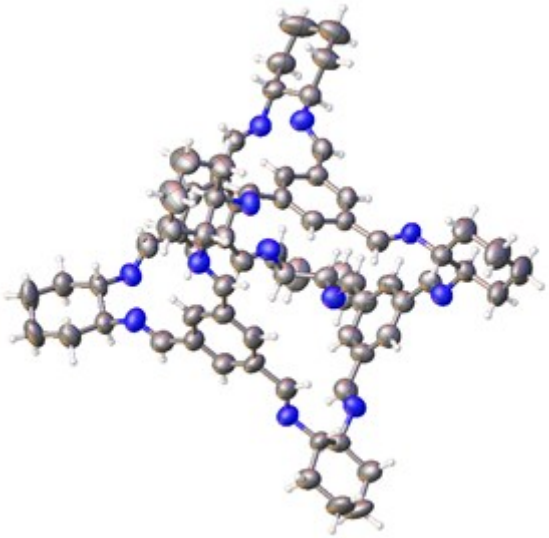

Figure S21. Displacement ellipsoid plot from the single crystal structure **CC3**-*RS*/**CC3**-*SR* recorded at 400(2) K showing one *R,R,R,S,S,S*-**CC3** cage in entirety. Ellipsoids displayed at 50 % probability level.

Following completion of the 400 K data set **CC3**-*RS*/**CC3**-*SR* was heated to 450 K (50 K/hr) and then to 500 K. Unit cells were determined at 10 K intervals during heating from 450 K to 500 K, **Table S2**.

Table S2. Variable temperature single crystal unit cell parameters determined for **CC3**-*RS*/**CC3**-*SR*, during heating to 500 K.

	450 K	**460 K**	**470 K**	**480 K**	**490 K**	**500 K**	**100 K[a]**
Crystal Class	Trigonal	Trigonal	Trigonal	Trigonal	Trigonal	Trigonal	Trigonal
***a* [Å]**	24.63(5)	24.75(5)	24.79(5)	24.75(4)	24.80(4)	24.77(5)	24.5032(12)
***c* [Å]**	19.80(4)	19.90(3)	19.95(3)	19.92(3)	19.94(3)	19.92(3)	19.6302(10)
***V* [Å^3]**	10410(40)	10550(40)	10620(40)	10570(30)	10620(30)	10580(40)	10207.1(11)

[a] Unit cell determined after cooling single crystal from 500 K to 100 K (330 K/hr).

Table S3. Solvated single crystal data for **CC3**-*RS*/**CC3**-*SR*

Crystallisation Solvent	Space Group	*a* [Å]	*c* [Å]	*V* [Å^3]
CH_2Cl_2/Acetone	$R\bar{3}$	24.412(2)	19.6184(19)	10125.4(16)
CH_2Cl_2/Et_2O	$R\bar{3}$	24.402(4)	19.527(3)	10070(3)

2.9 Powder X-ray Diffraction

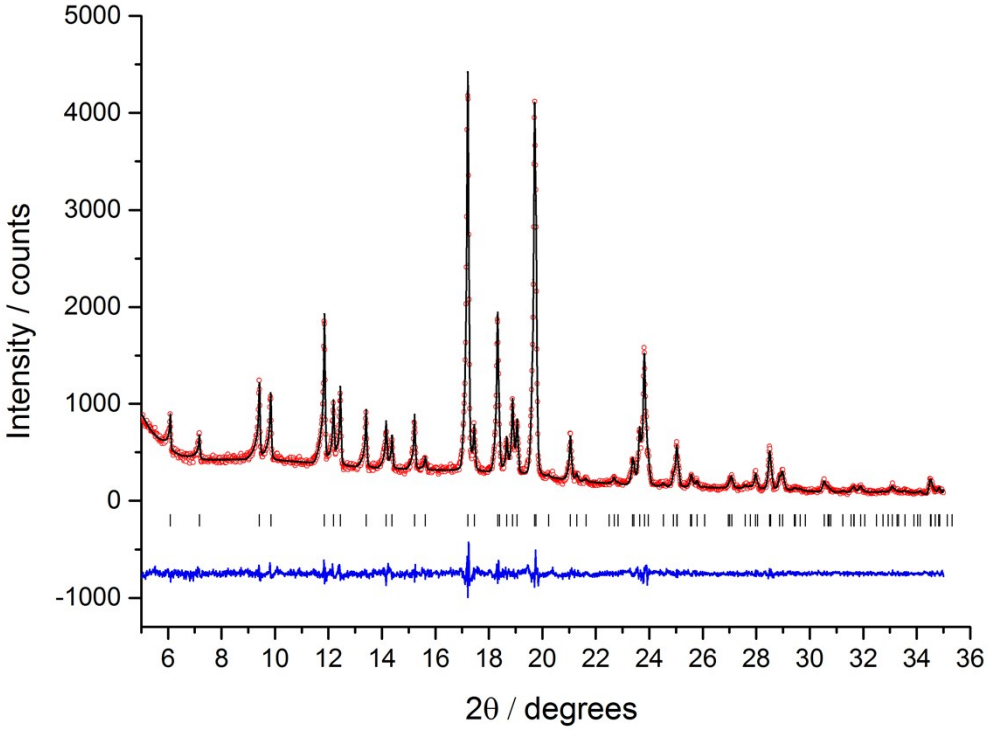

Figure S22. Le Bail fit for **CC3**-*RS*/**CC3**-*SR* recorded post gas sorption. Final observed (*red*), calculated (*black*) and difference (*blue*) PXRD profiles for Le Bail refinement (R_{wp} = 6.69%, R_p = 5.04 %, χ^2 = 1.27) of **CC3**-*RS*/**CC3**-*SR* (trigonal $R\bar{3}$, *a* = 24.6265(4) Å, *c* = 19.7952(6) Å; *V* = 10396.7(5) Å^3).

2.10 Gas Sorption

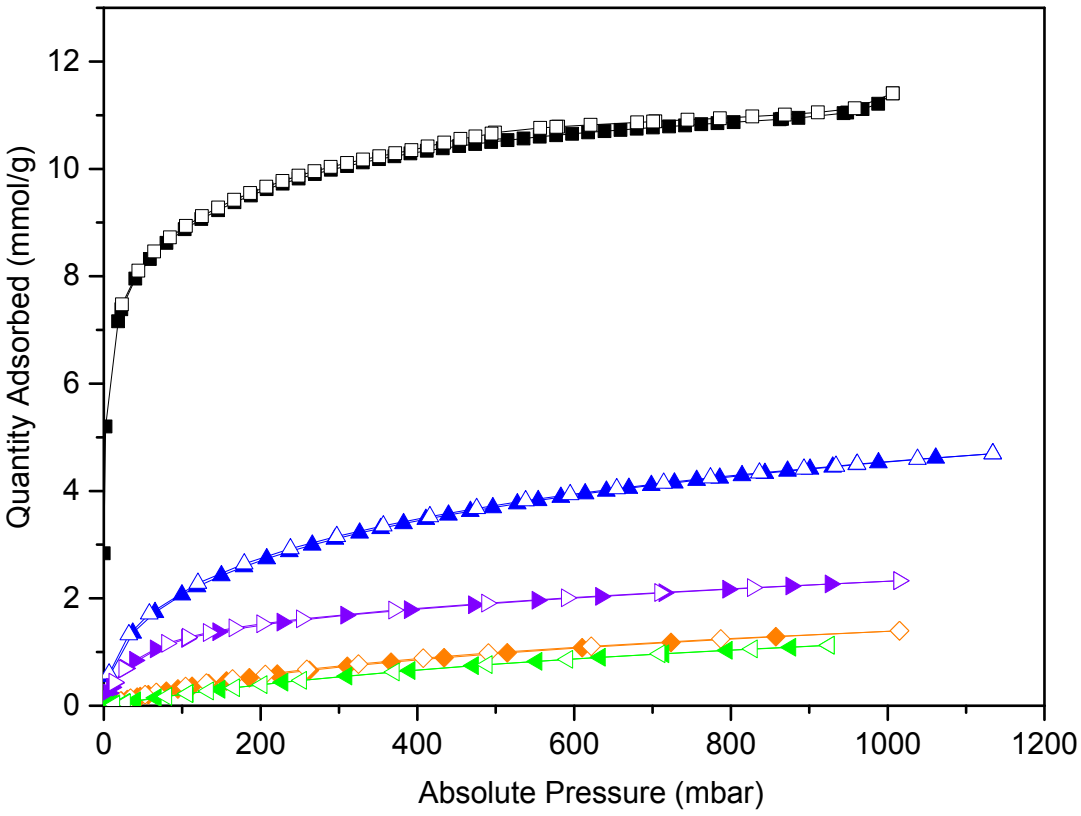

Figure S23. Gas sorption isotherms for N_2 (black, 77 K), H_2 (blue, 77 K), CO_2 (orange, 295 K), Xe (purple, 273 K), and Kr (green, 273 K) for **CC3**-*RS*/**CC3**-*SR*. Filled and open symbols represent adsorption and desorption isotherms, respectively. **(BET SA 800 m^2/g)**

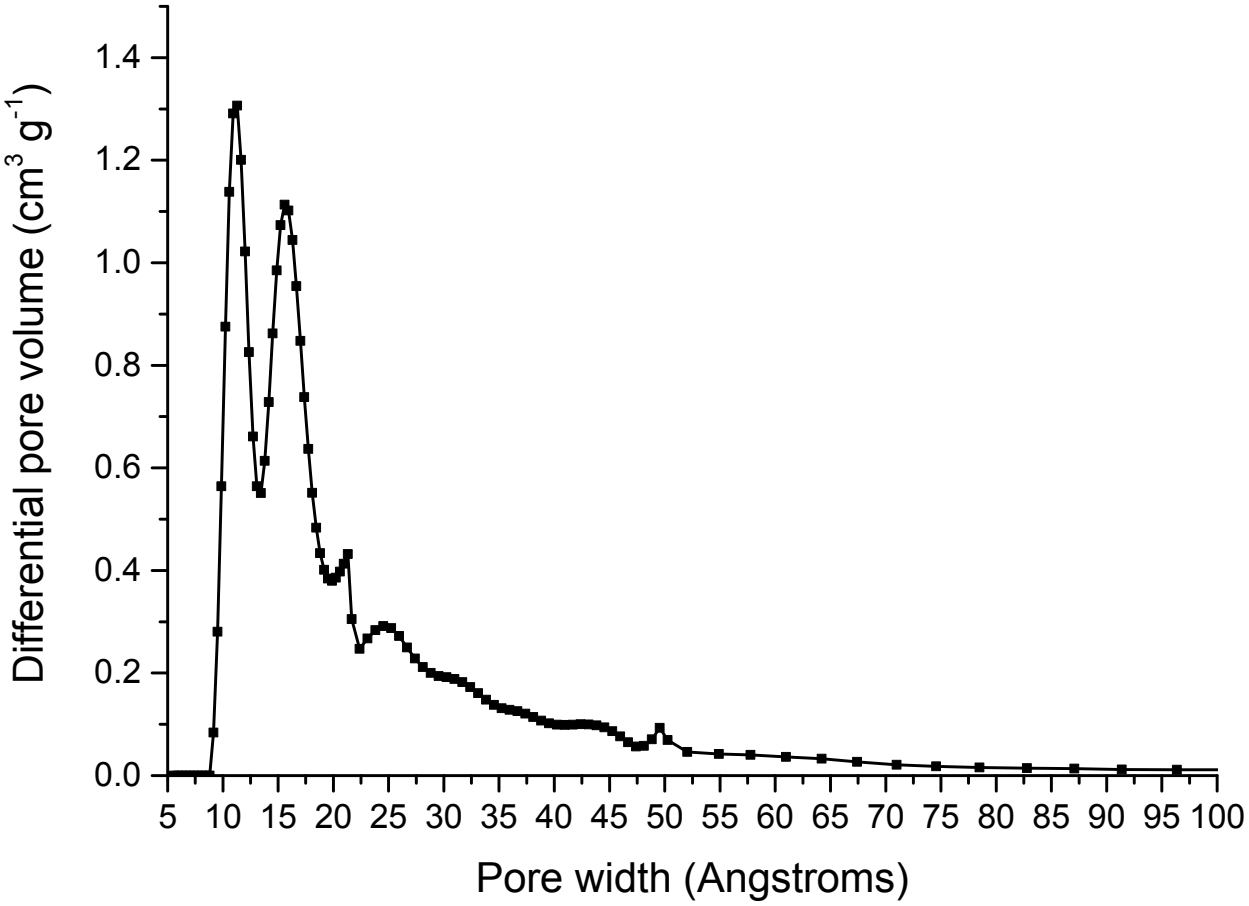

Figure S24. Differential pore size distributions for **CC3**-*RS*/**CC3**-*SR* derived from the N_2 isotherm in **Figure S23.** Values were calculated by application of hybrid density functional theory. Porosity predominately results from micropores (d < 2 nm), but a significant contribution from mesopores is observed (d > 2 nm). The bimodal distribution observed for **CC3**-*RS*/**CC3**-*SR* can be rationalised by examining the crystal structure; smaller micropores at ~ 1 nm arise from the pores within the cages, and larger micropores at ~ 1.6 nm arise from the void space between a pair of **CC3**-*RS* and **CC3**-*SR* cages. Very little extrinsic porosity is observed in the crystal structure, but the pore size distribution of the bulk sample is broad; this is consistent with the presence of defects due to reduced crystallinity resulting from the rapid precipitation of the sample, as seen for rapidly precipitated **CC3**-*R*.[8]

2.10 SEM Images

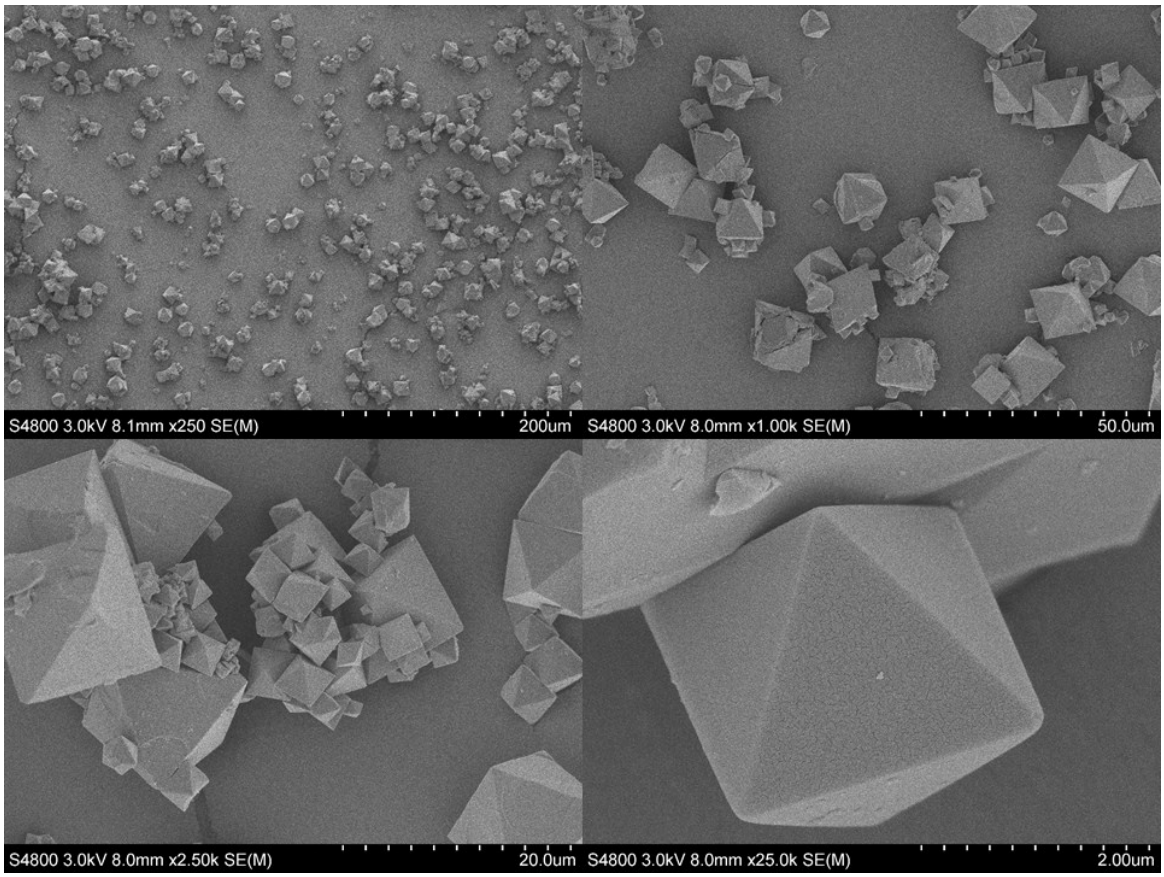

Figure S25. SEM images of **CC3**-*R*/**CC3**-*S* precipitate isolated from synthesis entry 5 (see table S1).

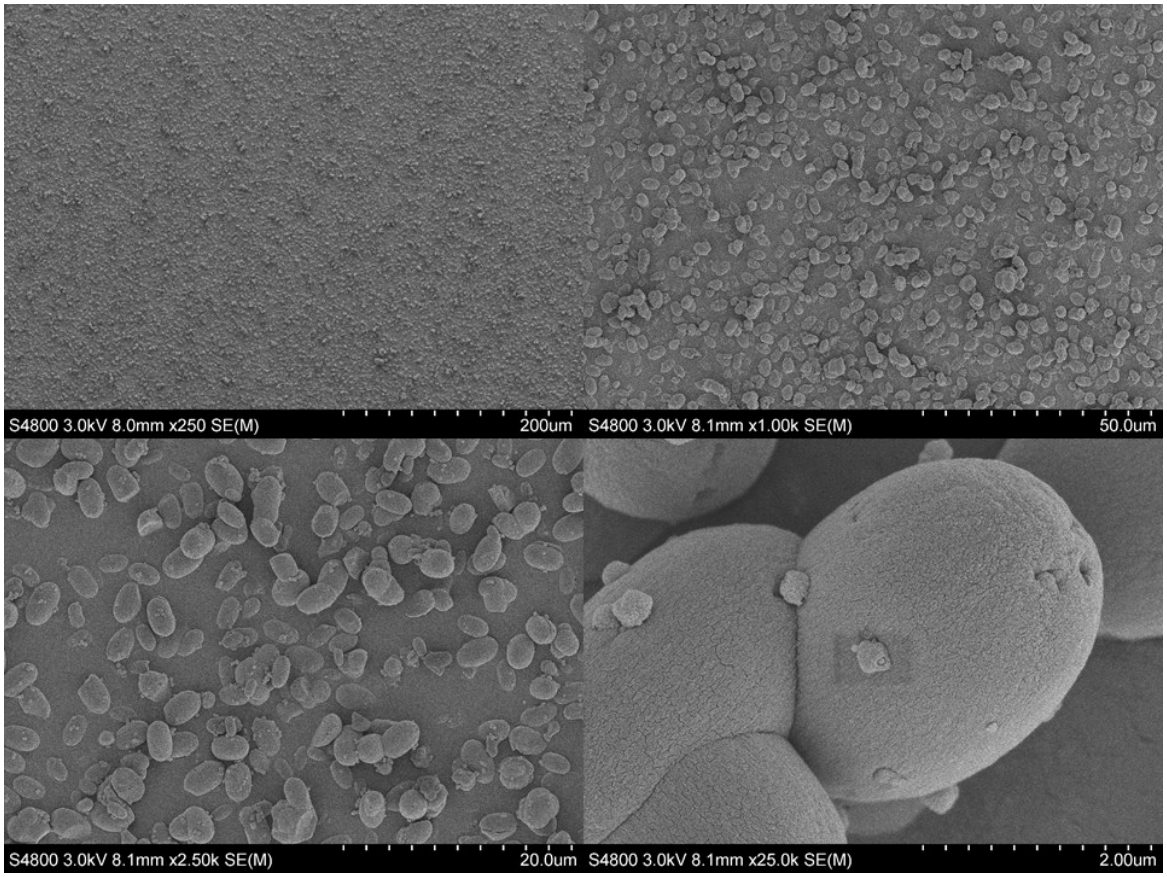

Figure S26: SEM images of **CC3**-*RS*/**CC3**-*SR* isolated from solution via precipitation with hexane in synthesis entry 5 (see table S1).

3.0 Computational details

Density functional theory calculations were performed in the mixed Gaussian and plane waves program CP2K/QUICKSTEP.[9,10] The isolated cage molecules for **CC3**-*R* and **CC3**-*RS* were taken from the single crystal X-ray diffraction structures (for **CC3**-*R* this is from CCDC 720850) and optimized in the gas phase. The PBE functional[11] with the molecularly optimised TZVP-MOLOPT basis sets[12] was used with the GTH-type pseudopotential,[13] a plane wave grid cutoff of 400 Ry and the Grimme-D3 dispersion correction.[13]

References

1. A. A. Coelho, 2007, TOPAS Academic. Version 4.1, Coelho Software.
2. S. Parsons, 2004, ECLIPSE. The University of Edinburgh, Edinburgh, UK.
3. G. M. Sheldrick, *University of Göttingen, Germany*, 2008.
4. G. M. Sheldrick, *Acta Cryst Sect A*, 2008, **64**, 112-122.
5. G. Sheldrick, *Acta Cryst Sect C*, 2015, **71**, 3-8.
6. O. V. Dolomanov, L. J. Bourhis, R. J. Gildea, J. A. K. Howard and H. Puschmann, *J Appl Cryst*, 2009, **42**, 339-341.
7. R. L. Greenaway, D. Holden, E. G. B. Eden, A. Stephenson, C. W. Yong, M. J. Bennison, T. Hasell, M. E. Briggs, S. L. James and A. I. Cooper, *Chem Sci*, 2017, **8**, 2640-2651.
8. T. Hasell, S. Y. Chong, K. E. Jelfs, D. J. Adams and A. I Cooper, *J Am Chem Soc,* 2012, **134**, 588-598.

9. J. VandeVondele, M. Krack, F. Mohamed, M. Parrinello, T. Chassaing and J. Hutter, *Comput Phys Commun*, 2005, **167**, 103-128.
10. The CP2K developers group: http://cp2k.berlios.de
11. J. P. Perdew, K. Burke and M. Ernzerhof, *Phys Rev Lett*, 1996, **77**, 3865-3868.
12. J. VandeVondele and J. Hutter, *J Chem Phys*, 2007, **127**.
13. S. Goedecker, M. Teter and J. Hutter, *Phys Rev B*, 1996, **54**, 1703-1710.
14. S. Grimme, J. Antony, S. Ehrlich and H. Krieg, *J Chem Phys*, 2010, **132**.